JGR Solid Earth

RESEARCH ARTICLE
10.1029/2018JB017093

Key Points:
- We analyze P wave peak displacements (Pd) of magnitude *M*4.5-9 earthquakes in Japan from 1997 to 2018
- Time-dependent saturation in the linear scaling between log10 Pd and magnitude is consistent with nondeterministic rupture
- We develop a Bayesian framework for rapid calculations of time-dependent uncertainties in real-time magnitude estimates

Supporting Information:
- Supporting Information S1
- Movie S1
- Movie S2

Correspondence to:
D. T. Trugman,
dtrugman@lanl.gov

Citation:
Trugman, D. T., Page, M. T., Minson, S. E., & Cochran, E. S. (2019). Peak ground displacement saturates exactly when expected: Implications for earthquake early warning. *Journal of Geophysical Research: Solid Earth*, *124*. https://doi.org/10.1029/2018JB017093

Received 27 NOV 2018
Accepted 11 APR 2019
Accepted article online 16 APR 2019

Peak Ground Displacement Saturates Exactly When Expected: Implications for Earthquake Early Warning

Daniel T. Trugman[1], Morgan T. Page[2], Sarah E. Minson[3], and Elizabeth S. Cochran[2]

[1]Los Alamos National Laboratory, Los Alamos, NM, USA, [2]US Geological Survey, Pasadena, CA, USA, [3]US Geological Survey, Menlo Park, CA, USA

Abstract The scaling of rupture properties with magnitude is of critical importance to earthquake early warning systems that rely on source characterization using limited snapshots of waveform data. ShakeAlert, a prototype earthquake early warning system that is being developed for the western United States, provides real-time estimates of earthquake magnitude based on *P* wave peak ground displacements measured at stations triggered by the event. The algorithms used in ShakeAlert assume that the displacement measurements at each station are statistically independent and that there exists a linear and time-independent relation between log peak ground displacement and earthquake magnitude. Here we challenge this basic assumption using the largest data set assembled for this purpose to date: a comprehensive database of more than 140,000 vertical-component waveforms from M4.5 to M9 earthquakes occurring near Japan from 1997 through 2018 and recorded by the K-NET and KiK-net strong-motion networks. By analyzing the time evolution of *P* wave peak ground displacements for these earthquakes, we show that there is a break, or saturation, in the magnitude-displacement scaling that depends on the length of the measurement time window. We demonstrate that the magnitude at which this saturation occurs is well-explained by a simple and nondeterministic model of earthquake rupture growth. We then use the predictions of this saturation model to develop a Bayesian framework for estimating posterior uncertainties in real-time magnitude estimates.

1. Introduction

Do earthquakes large and small begin alike, or are there systematic differences in the early rupture process that distinguish them? This question drives at the core of our knowledge of how earthquakes nucleate, rupture, and arrest and remains one of the crucial unresolved questions in seismology. Following the pioneering work of Aki (1967), the notion of self-similar scaling of earthquake rupture properties became the prevailing conceptual paradigm. This framework was supported by the nearly constant distribution of earthquake stress drop and scaled energy spanning many orders of magnitude (e.g., Ide & Beroza, 2001). Likewise, computational models of self-similar crack-like ruptures can be used to explain many of the key characteristics of observed seismic waveform spectra (Brune, 1970; Eshelby, 1957; Madariaga, 1978). Despite this success, the rupture processes of real earthquakes deviate from the behavior of self-similar cracks in several notable ways. Large earthquakes, for example, are geometrically constrained by the finite width of the seismogenic zone (Denolle & Shearer, 2016; Gomberg et al., 2016), activate dynamic frictional weakening processes that strongly influence rupture propagation (Brodsky & Kanamori, 2001; Goldsby & Tullis, 2011; Noda & Lapusta, 2013), and may favor pulse-like rather than crack-like rupture modes (Heaton, 1990; Melgar & Hayes, 2017). While these observations differ from classical notions of self-similarity, they do not necessarily imply that systematic differences in the early rupture processes of earthquakes determine the final earthquake size.

This question of rupture determinism is of direct relevance to earthquake early warning (EEW) systems that require rapid earthquake source characterization in order to issue accurate and timely alerts of strong shaking (Minson et al., 2018). If the ultimate size of an earthquake is determined by its initial energy budget (Ellsworth & Beroza, 1995; Nielsen, 2007), then it may be possible to assimilate this information to rapidly forecast the final earthquake magnitude while the rupture is still in progress (Allen & Kanamori, 2003; Colombelli et al., 2014; Olson & Allen, 2005; Zollo et al., 2006). Observations of large and great earthquakes

in recent years have challenged this view of rupture determinism (Rydelek & Horiuchi, 2006; Rydelek et al., 2007; Yamada & Ide, 2008). Meier et al. (2016) examined near-source peak displacement measurements, finding no evidence for differences in the rupture onsets of small and large earthquakes, and Meier et al. (2017) showed that the source time functions of large earthquakes follow a universal, nondeterministic time evolution. Kanamori (2005) documented the potential for EEW parameters collected over short time windows to saturate at large magnitudes, implying that the measurements from early in the rupture process do not predetermine the final earthquake size. This observation was further reinforced by the severe underestimates of the final size of 2011 M9.0 Tohoku-Oki earthquake by made EEW systems (Colombelli et al., 2012; Hoshiba & Iwakiri, 2011). More recently, Leyton et al. (2018) analyzed seismic and geodetic waveforms from earthquakes in the Chilean subduction zone, finding that EEW source characterization can be significantly improved using extended measurement time windows, which is inconsistent with the notion of rupture determinism. While these studies suggest that a purely deterministic rupture mechanism can likely be ruled out, a weak or probabilistic form of determinism may still be observed in some instances through careful analysis of seismic or geodetic data (Goldberg et al., 2019; Melgar & Hayes, 2017; Olson & Allen, 2006).

This study builds on these observations by examining the question of rupture determinism and its implications from the perspective of the ShakeAlert system, which is currently being tested prior to its implementation in the western United States (Cochran et al., 2018; Kohler et al., 2018). We focus in particular on the time evolution of seismically recorded peak ground displacement (P_d), a key parameter in the ShakeAlert system whose accurate measurement is central to its real-time point-source characterization algorithm (Chung et al., 2019; Kuyuk et al., 2014). We emulate ShakeAlert's waveform processing workflow for an off-line, comprehensive data set of more than 140,000 waveforms recorded by Japan's K-NET and KiK-net strong-motion networks. This data set is to our knowledge the largest assembled for this purpose to date. It includes 2,409 magnitude 4.5–9.0 earthquakes in total, with 151 M6 and 22 M7 and greater earthquakes that provide robust assessments of how EEW parameters like P_d scale with magnitude. We measure vertical-component, *P* wave P_d in progressively longer time windows preceding the *S* wave arrival and show there is a time-dependent saturation in the assumed linear relation between $\log_{10}P_d$ and magnitude *M* that is well-predicted by a simple and nondeterministic rupture model. With this saturation model in hand, we develop a novel Bayesian framework for estimating posterior uncertainties in real-time magnitude estimates that account for the saturation effect inherent in the use of limited measurement time windows. We conclude by discussing the scientific and practical implications of our key contributions to the existing literature: careful measurements of time-dependent saturation of P_d in a massive data set of M4.5–M9 earthquakes and a Bayesian workflow for computing time-dependent uncertainties in early warning magnitude estimates.

2. Methods: Data Set Overview and Waveform Processing

We focus our analysis on earthquakes with magnitude $M \geq 4.5$ and hypocentral depths ≤100 km occurring from October 1997 through December 2018 in a rectangular region surrounding Japan (Figure 1). For each earthquake, we select all available vertical-component waveforms recorded at K-NET and KiK-net surface stations with epicentral distance $R_{\text{epi}} \leq 200$ km. K-NET and KiK-net are the National Research Institute for Earth Science and Disaster Resilience's two premier strong-motion accelerometer networks, composed of more than 1,700 stations located onshore Japan and with typical station spacing of less than 20 km. Triggered waveforms are archived by the National Research Institute for Earth Science and Disaster Resilience and are publicly available upon request. It is important to note that since our analysis is limited to an off-line database of triggered waveforms, the results we present here likely underestimate the true uncertainties that would be expected for real-time EEW systems, where location errors and false event triggers are more common.

Our waveform processing procedure closely emulates that of the ShakeAlert system, deviating only where necessary to accommodate differences in the network and source-station geometry between the western United States and Japan (e.g., Nof & Allen, 2016; see supporting information Text S1 for further details). For each waveform, we estimate the *P* wave onset time using a modified form of the automatic triggering algorithm proposed by Allen (1978), which triggers when the ratio of the short-term average to long-term average of a characteristic function of acceleration and velocity time series exceeds a specified threshold. To mitigate spurious triggers caused by occasional noise spikes, we additionally require that the peak acceleration amplitude exceeds 0.1 cm/s^2 in a 3-s window following the triggered arrival time. We further consider

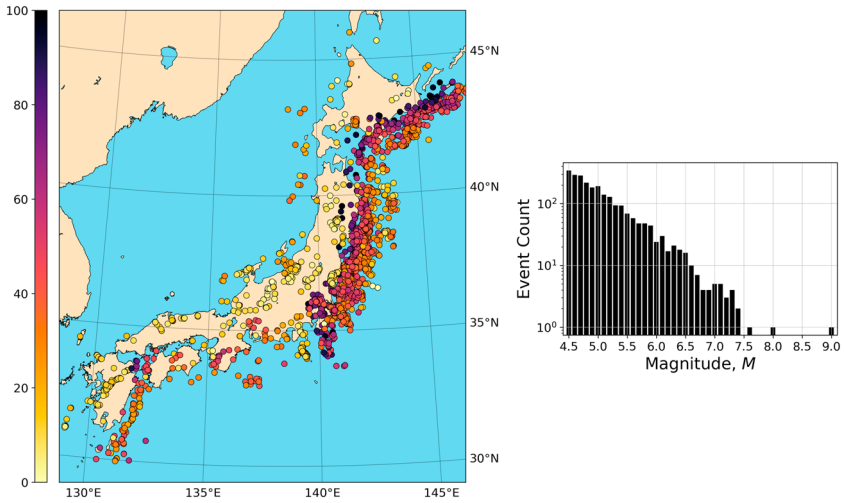

Figure 1. Map of the study region and corresponding magnitude histogram (log-scale). Our data set includes earthquakes with magnitude $M \geq 4.5$ and hypocentral depths ≤ 100 km occurring from 1997 through 2018. Latitude and longitude boundaries are [30.0°N,46.0°N] and [129.0°E,149.0°E], respectively. Earthquakes in the study region map (left) are color-coded by hypocentral depth. Most earthquakes in the data set have Japan Meteorological Agency magnitudes ranging from 4.5 to 7.6, with one M8 and one M9 event (right).

only the subset of earthquakes with at least four waveform records with $R_{\text{epi}} \leq 200$ km that meet these quality control criteria. In total, our data set consists of 140,528 vertical-component records derived from 2,409 earthquakes with magnitudes ranging from 4.5 to 9.0 (Figure S1).

Real-time magnitude estimates from the point-source algorithm in the ShakeAlert system are based primarily on peak ground displacements, P_d, measured from P waveforms on vertical-component channels (Brown et al., 2011; Chung et al., 2019; Kohler et al., 2018; Kuyuk & Allen, 2013). Rather than focus on a fixed time measurement time window TW, we compute P_d continuously in time following the P wave onset (Figure 2). To do so, we first demean and apply a gain correction to each K-NET and KiK-net acceleration waveform. We then apply a causal, four-pole Butterworth high-pass filter with a corner at 0.075 Hz to remove long-period trends and noise and integrate these processed acceleration waveforms to velocity and then to displacement. We apply a 0.075- to 3.0-Hz band-pass filter to each displacement record and measure the peak displacement amplitude P_d at each sampling time step following the P wave arrival. Finally,

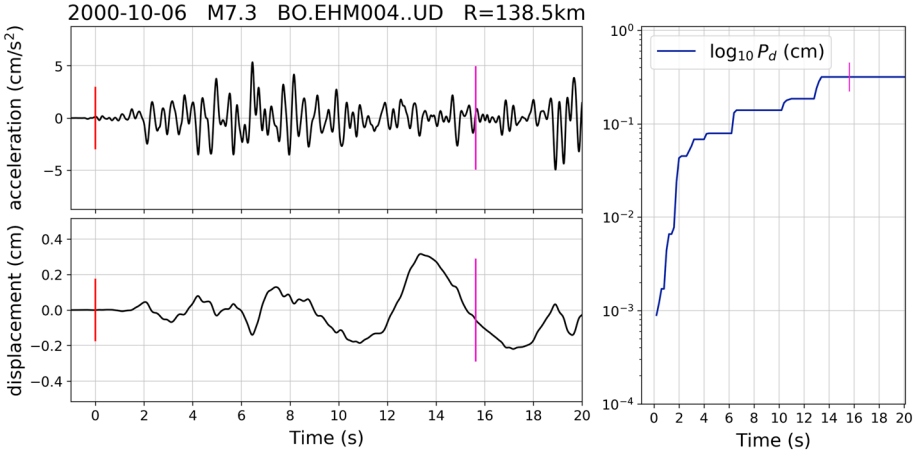

Figure 2. Example of the waveform processing for a M7.3 earthquake occurring in October 2000 and recorded at station EHM004 ($R_{\text{epi}} = 138.5$ km). The P wave onset is determined on the acceleration waveform (top left) using a modified form of the Allen (1978) triggering algorithm. Peak displacement P_d (right) is measured continuously in time relative to the P wave arrival based on the doubly integrated displacement record (bottom left). P_d measurements are truncated at the 95% of the theoretical S wave arrival (vertical purple line) to prevent measurements of S wave displacements.

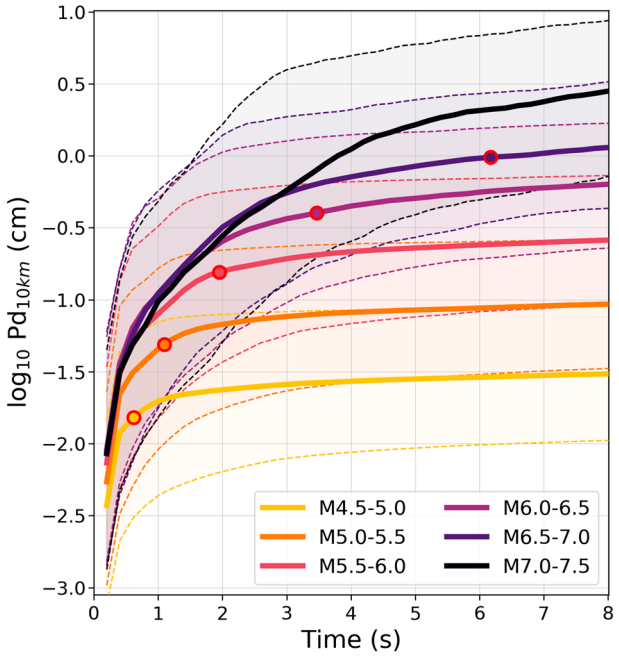

Figure 3. Time evolution of log peak displacement $\log_{10}P_d$ for different magnitude earthquakes. Median values of $\log_{10}P_d$ (solid lines) in six magnitude bins ranging from 4.5 to 7.5 are normalized to 10-km epicentral distance and plotted as a function of time. The shaded envelopes enclosed by dashed lines correspond to the 20–80% percentile range of records in each magnitude bin. The mean expected rupture duration for each bin (assuming 2.0-MPa stress drop) is marked with a red circle.

we truncate the P_d measurements at the value measured at 95% of the theoretical *S*-minus-*P* time (Ueno et al., 2002) to avoid measurement of *S* wave displacements and normalize each P_d measurement to 10-km epicentral distance using the global regression relation of Kuyuk and Allen (2013). This normalization provides a first-order correction for distance attenuation in P_d, though does neglect variations in event depth that may be important in the near-source region. We also acknowledge that the frequency sensitivity of the accelerometers, when combined with this filtering and integration procedure, may in some instances provide biased estimates of the true peak ground displacement (e.g., Crowell et al., 2012; Melgar et al., 2013, see section 4 for further discussion). Since the double integration of the waveforms effectively acts as a low-pass filter, the results presented here are not very sensitive to the choice of the 3 Hz upper corner that we use for consistency with previous studies.

3. Results

We first assess evidence for and against a deterministic rupture model in which there are measurable and systematic differences in the rupture onset of earthquakes that control the final earthquake size (Olson & Allen, 2005). To do this, we plot the time evolution of P_d for different magnitude bins (Figure 3). The median values of P_d in each magnitude bin follow a universal pattern of steep initial power law growth (Meier et al., 2016) before leveling off at time that scales with expected rupture duration. The time evolution of these growth curves indicates that we are unlikely to be able to distinguish between the earthquakes of different sizes while the rupture is still growing. While it is possible that there exist alternative statistical features of waveforms that can more rapidly estimate earthquake magnitude, these results suggest that EEW systems that rely on P_d cannot presume the validity of rupture determinism.

An implication of nondeterministic rupture is that when computing EEW parameters like P_d, the duration of the measurement time window *TW* can matter a great deal. EEW systems that estimate *M* using P_d assume a linear regression relation of the form:

$$\log_{10}P_d(M) = c_0 + c_1 M, \tag{1}$$

where P_d is distance-corrected and c_0 and c_1 are empirical regression coefficients. The basis of this relation is that in the far field, P_d should be proportional to the rate of moment release (Aki & Richards, 2002), but the true value of P_d is only achieved once the moment rate function peaks. If the rupture duration T_{rup} is less than *TW*, then there should be a linear scaling between magnitude *M* and $\log_{10}P_d$, as is assumed by ShakeAlert and other comparable systems. Conversely, if T_{rup} exceeds *TW*, then measured P_d values saturate and are independent of *M*.

We can account for this nonlinear time dependence in P_d measurements using a simple model of earthquake rupture to derive the relation between T_{rup} and *M* for a given value of earthquake stress drop $\Delta\sigma$. We assume a bilateral rupture with constant velocity V_{rup} in which the rupture transitions from 2-D circular growth to 1-D elliptical growth once the rupture front reaches the width of the seismogenic zone *W* (Gomberg et al., 2016). In this study, we use a fixed value for *W* of 50 km, which seems an appropriate compromise for the mixture of crustal and subduction zone earthquakes that occur in Japan, though we do not have enough $M \gtrsim 7.5$ earthquakes to test this directly. Under these assumptions, the relation between *M* and $\log_{10}T_{\text{rup}}$ is piecewise linear, with the hingepoint occurring at the transition time from 2-D to 1-D rupture propagation, $T_X = W/2V_{\text{rup}}$. Measuring V_{rup} in kilometers per second and $\Delta\sigma$ in megapascals, the scaling relations between *M* and $\log_{10}T_{\text{rup}}$ in these regimes have slopes of 2 and 2/3:

$$\begin{aligned} T_{\text{rup}} < T_X &: \; M = 2\log_{10}T_{\text{rup}} + \frac{2}{3}\left[\log_{10}\left(\frac{16}{7}\Delta\sigma V_{\text{rup}}^3\right) - 9.1\right] \\ T_{\text{rup}} > T_X &: \; M = \frac{2}{3}\log_{10}T_{\text{rup}} + \frac{2}{3}\left[\log_{10}\left(\frac{16}{7}\Delta\sigma V_{\text{rup}}^3\right) - 9.1\right] + \frac{4}{3}\log_{10}T_X. \end{aligned} \tag{2}$$

Applying (2), we can see that the magnitude at which saturation is expected to occur depends on the assumed values of $\Delta\sigma$ and V_{rup}, with higher values leading to shorter rupture durations. Because earthquakes exhibit a range of $\Delta\sigma$ and V_{rup} values, the saturation of P_d measurements occurs gradually with magnitude rather than abruptly.

With these concepts in mind, we can generalize (1) to account for magnitude saturation by introducing the concept of the survival function:

$$S(TW|M) = \mathbf{P}(TW > T_{Pd}|M), \tag{3}$$

that is, the probability $\mathbf{P}$ that the measurement TW exceeds the time at which the true P_d is recorded for an earthquake with magnitude M. The survival function is commonly used in statistics (it is equal to one minus the cumulative probability density function), and in this context allows us to account for the natural variability in rupture duration for earthquakes of a given magnitude. For the purposes of this study, we compute S by taking advantage of the observations that (i) source time functions are peaked such that $T_{Pd} \lesssim T_{\text{rup}}/2$ (e.g, Meier et al., 2017) and (ii) earthquake stress drop values measured in log units closely follow a normal distribution (e.g., Allmann & Shearer, 2009; Trugman & Shearer, 2017). This simplifies S to the survival function of a normal distribution, and the revised saturation model can be related to the integral of S:

$$\log_{10}P_d(M\,|\,TW) = c_0 + c_1 \int_0^M S(\Delta\sigma^*_{TW}|M')\,\mathrm{d}M'. \tag{4}$$

Here the survival function

$$S(\Delta\sigma_{TW}|M) = \mathbf{P}(\Delta\sigma < \Delta\sigma^*_{TW}|M) \tag{5}$$

has been reformulated to give the probability that the stress drop $\Delta\sigma$ of a given earthquake is less than the critical value $\Delta\sigma^*_{TW}$ of an event with magnitude M and $T_{\text{rup}} = 2\,T_{Pd} = 2\,TW$.

In Figure 4, we plot distance-corrected $\log_{10}P_d$ versus M for measurement TW ranging from 1 to 20 s and compare with saturation model predictions (equation (4), red curves). Overall, the data are well-explained by (4), where for simplicity, we have fixed V_{rup} to 2.5 km/s, which is typical of values listed in the literature (e.g., Ye et al., 2016), and have accounted for variability in T_{rup} by assuming a lognormal distribution of $\Delta\sigma$ with a 2-MPa mean and a $\log_{10}$ standard deviation of 0.5. While our data set does not have much resolution above M7.5, the smooth transition from linear to M-independent scaling of $\log_{10}P_d$ predicted by our model is consistent with the available observations. For shorter TW, the M9 Tohoku-oki earthquake is a notable outlier, while the second largest earthquake, the 2003 M8 Tokachi-oki earthquake, is not. We address this further in section 4.

In real-time EEW scenarios, the situation is reversed from that shown in Figure 4: Given an event-averaged set of P_d measurements, what is the magnitude of the earthquake? We can use our saturation model (4) in combination with Bayes rule to provide a quantitative answer to this question. To do so, we need to rewrite (4) in the form of a data likelihood function $\mathbf{P}(\log_{10}P_d\,|\,M)$ and assume a prior for the magnitude distribution $\mathbf{P}(M)$. Then Bayes rule can be applied to estimate the posterior magnitude distribution consistent with the available observations and our prior assumptions:

$$\mathbf{P}(M\,|\,\log_{10}P_d, TW) \propto \mathbf{P}(\log_{10}P_d|M, TW)\,\mathbf{P}(M), \tag{6}$$

where the constant of proportionality can be obtain through proper normalization of the posterior probability distribution $\mathbf{P}(M\,|\,\log_{10}P_d, TW)$.

In this study, we apply simple functional forms for the likelihood and prior probability distributions to enable rapid, analytic estimates of the posterior distribution. In particular, we assume a prior distribution based on a Gutenberg-Richter (GR) power law of the form $\mathbf{P}(M) \sim 10^{-M}$, which closely captures the underlying magnitude distribution of our earthquake data set (and that of most others comparable to it). For the likelihood function $\mathbf{P}(\log_{10}P_d|M, TW)$, we assume a normal distribution for the event-averaged $\log_{10}P_d$ with the mean of the distribution given by our saturation model (4) and the variance τ^2 that depends on the between-event and within-event variability, τ^2_{BE} and τ^2_{WE}, and the number of triggered stations N:

$$\tau^2 = \tau^2_{\text{BE}} + \tau^2_{\text{WE}}/N. \tag{7}$$

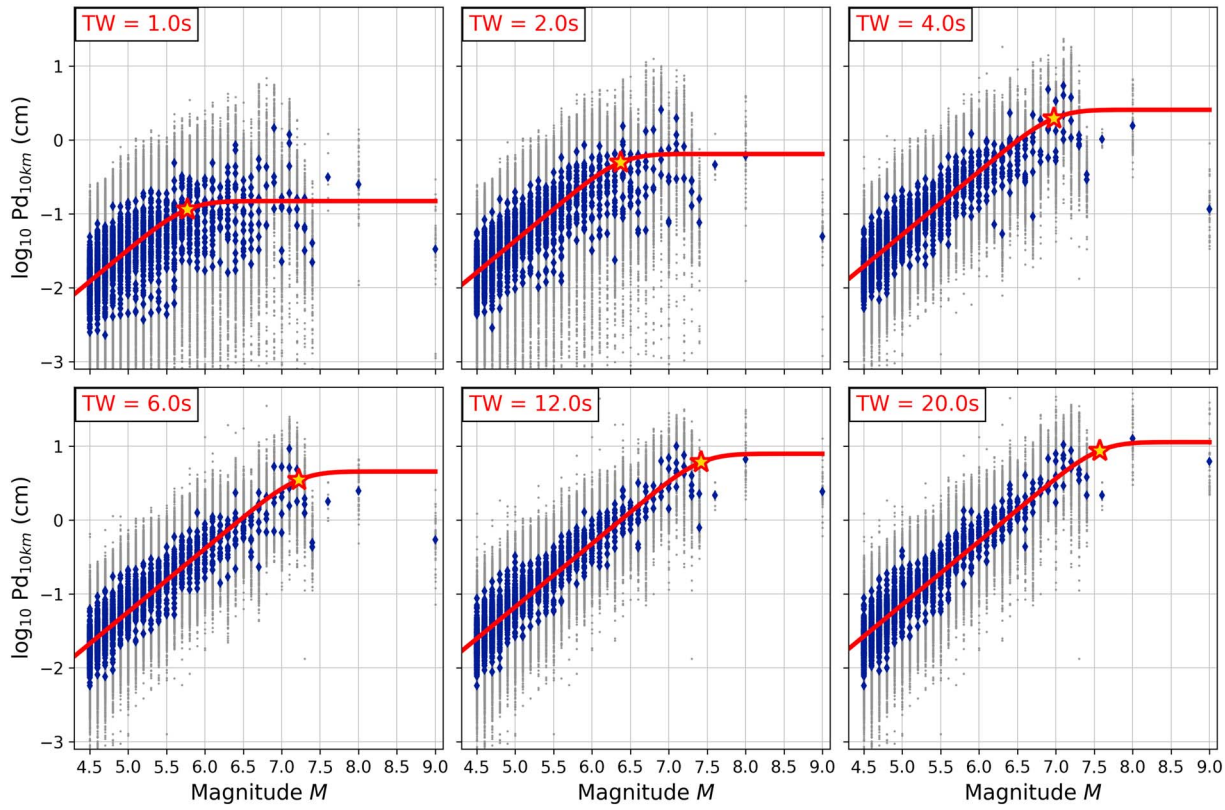

Figure 4. Log peak displacement $\log_{10}P_d$ versus magnitude M and comparison to saturation model predictions. Each panel shows a different measurement time window length (TW), with values increasing from 1 (upper left) to 20 s (lower right). Individual records of $\log_{10}P_d$ are corrected to 10-km epicentral distance and marked as gray dots, and event-averaged $\log_{10}P_d$ are marked with blue diamonds. Saturation model predictions for each TW (equation (4)) are marked with solid red lines. The saturation magnitude marking the midpoint of the transition from linear to M-independent scaling increases with increasing TW length (gold stars).

This functional form is supported by the observation that both the between-event and within-event variability in $\log_{10}P_d$ closely follow normal distributions whose standard deviations decrease with increasing TW (Figure S2) but do not appear to vary significantly with magnitude.

This basic approach allows us to rapidly estimate posterior probabilities for earthquake magnitude, given a set of real-time P_d measurements. In Figures 5 and 6, we show the results of applying (6) to our data set, using the same set of observations and time windows shown in Figure 4 (see Movies S1 and S2 for the full time evolution). For each time window, we plot the likelihood distribution (Figure 5) and associated posterior probability distribution (Figure 6) for a range of different $\log_{10}P_d$ measurements. These results illustrate that the length of measurement TW has a fundamental impact on the uncertainties in the magnitude estimate. Shorter time windows lead to larger posterior uncertainties, and the posterior distributions become highly asymmetric as the measured P_d value approaches the saturation value given by (4). In these instances, $\log_{10}P_d$ provides only a lower bound on the range of plausible earthquake magnitudes due to the potential for the rupture to keep growing and for the final T_{rup} to exceed TW. For a fixed TW, increasing the number of measurements N (e.g., through denser station coverage) reduces the posterior uncertainties (Figure S3) because the uncertainty of the mean $\log_{10}P_d$ estimate for each event is reduced by a factor of $\sqrt{N}$. This reduction in uncertainty, while certainly desirable, is however limited because improvements to station coverage cannot be used to overcome the inherent uncertainties of between-event variability or the use of short measurement TWs. Further, this also assumes that each station provides a statistically independent measurement, which is overly optimistic given the spatial correlation of nearby stations.

One useful aspect of this formulation is that it allows us to quantify how long the measurement TW needs to be in order to distinguish between earthquakes of different sizes. In Figure 7, we show the expected time evolution of the posterior magnitude distribution for earthquakes with magnitudes ranging from 5 to 8. For smaller earthquakes ($M \leq 5$), measurement TW of 2 s or less may be sufficient. Distinguishing between M6

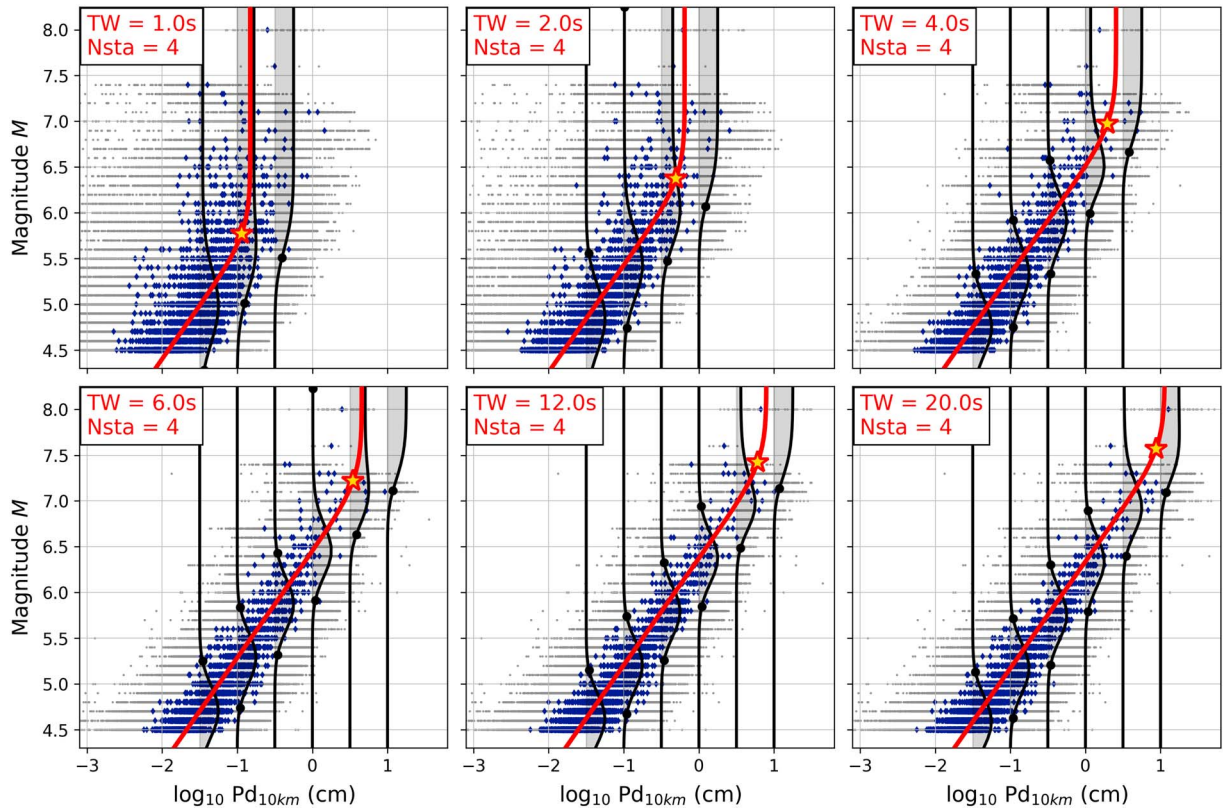

Figure 5. Magnitude M versus log peak displacement $\log_{10}P_d$ and comparison to the likelihood distribution. Each panel shows a different measurement time window length (TW), with values increasing from 1 (upper left) to 20 s (lower right). Individual records of $\log_{10}P_d$ records are corrected to 10-km epicentral distance and marked as gray dots, and event-averaged $\log_{10}P_d$ are marked with blue diamonds. Mean predictions from the likelihood function for each TW are marked with solid red lines, and the saturation magnitude is marked with a gold star. The shaded regions correspond to likelihood probability distributions $\mathbf{P}(\log_{10}P_d|M,TW)$ for $\log_{10}P_d$ values ranging from −1.5 to 1.0, with circular markers denoting endpoints of the 95% credibility interval. The calculations assume $N = 4$ observations per event.

and M7 or larger takes longer, of order 5 s or more. And for the largest earthquakes, measurement TWs in excess of 20 s are likely needed.

4. Discussion

To summarize, the novel contributions of this study include (1) a careful confirmation and quantification of the time-dependent magnitude saturation of peak displacement P_d using the largest data set assembled for this purpose to date, (2) connection of P_d saturation to magnitude uncertainty in EEW systems, and (3) development of a Bayesian approach to rapidly calculate time-dependent uncertainties for P_d-based magnitude estimates. While this Bayesian formulation has a physically sound basis supported by observations of nondeterministic rupture evolution, it does include a number of simplifying assumptions about earthquake rupture. Real earthquakes exhibit a rich variety of rupture behavior that deviate from our simple model, with variations in rupture velocity, fault geometry (and associated seismogenic width), and rupture mode (pulse-like vs. crack-like) being notable examples. However, this natural variability is accounted for within the context of our model by allowing for a range of plausible stress drop values, which in turn allows for a range in plausible rupture durations for earthquakes of a given magnitude. Further, this framework provides a computationally efficient means of rigorously accounting for uncertainties in P_d-based magnitude estimates and how they evolve with time and with different numbers of observations. For real-time calculations, stations within the recording network will trigger at different times depending on the relative source-station distances. At any given time, stations closer to the source will have recorded longer and hence have lower magnitude uncertainties. This information could in principle be used in a Bayesian weighting scheme to more accurately aggregate the real-time magnitude estimates from individual stations. Further research is needed, however, to understand how best to ensure that these time-dependent uncertainties in earthquake

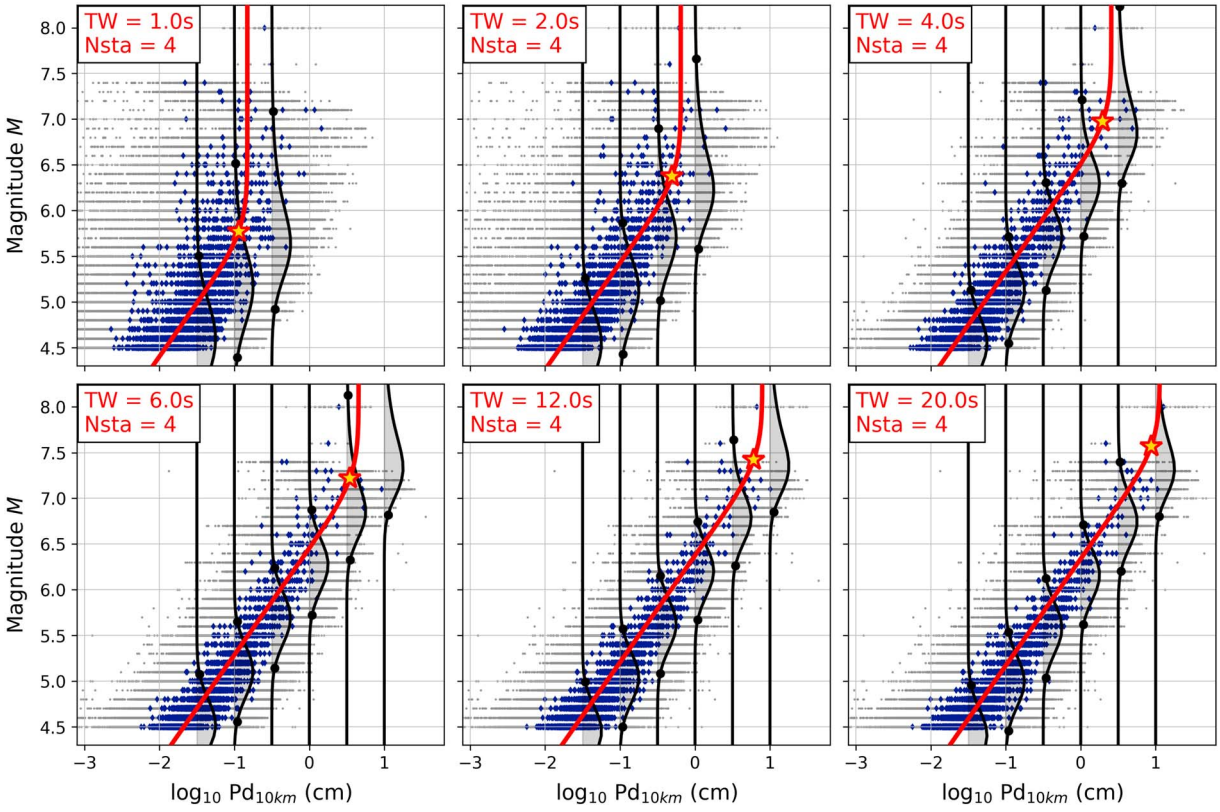

Figure 6. Magnitude M versus log peak displacement $\log_{10}P_d$ and associated posterior uncertainties. Each panel shows a different measurement time window length (TW), with values increasing from 1 (upper left) to 20 s (lower right). Individual records of $\log_{10}P_d$ are corrected to 10-km epicentral distance and marked as gray dots, and event-averaged $\log_{10}P_d$ are marked with blue diamonds. Mean predictions from the likelihood function for each TW are marked with solid red lines, and the saturation magnitude is marked with a gold star. The shaded regions correspond to posterior probability distributions $\mathbf{P}(M\,|\log_{10}P_d, TW)$ for $\log_{10}P_d$ values ranging from −1.5 to 1.0, with circular markers denoting endpoints of the 95% credibility interval. The calculations assume a Gutenberg-Richter prior $\mathbf{P}(M) \sim 10^{-M}$ and $N = 4$ observations per event.

magnitude are fully propagated into the ground-motion prediction equations and resulting alert messages produced by EEW systems.

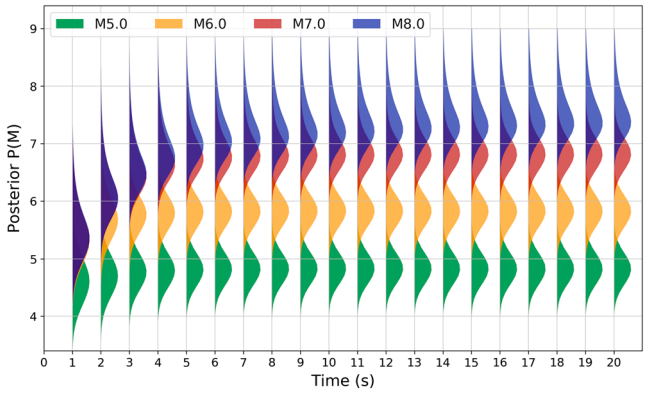

Figure 7. Expected time evolution of the posterior magnitude estimates for earthquakes of different sizes. The posterior probability distribution for typical magnitude 5 (green), magnitude 6 (yellow), magnitude 7 (red), and magnitude 8 (blue) earthquakes are displayed vertically as a function of measurement time window, assuming $N = 4$ observations per event.

In our Bayesian formulation, the posterior distribution $\mathbf{P}(M\,|\log_{10}P_d, TW)$ is to some degree sensitive to our prior assumptions about the magnitude distribution $\mathbf{P}(M)$. In this study, we use a GR prior $\mathbf{P}(M) \sim 10^{-M}$, which is applicable to a wide range of contexts in seismology and captures the underlying magnitude distribution of our data set. Assuming a GR prior allows the posterior distribution to closely match the underlying data, which has many more small earthquakes than large ones. Indeed, the prior distribution provides the only constraint on the posterior estimates at large magnitudes once the saturation point in P_d has been exceeded (Figure 8). It should be noted, however, that the using a GR prior has the effect of reducing the expected M for a given set of P_d observations, relative to uniform prior $\mathbf{P}(M)$, where the posterior distribution is directly proportional to the likelihood function. This may be undesirable for certain uses of EEW in which an underestimate of M is more consequential than an overestimate of comparable scale (e.g., Meier, 2017). However, in our view the objective of the EEW system itself should be to provide an unbiased estimate of the posterior distribution, rather than a biased one that employs an unrealistic uniform magnitude prior.

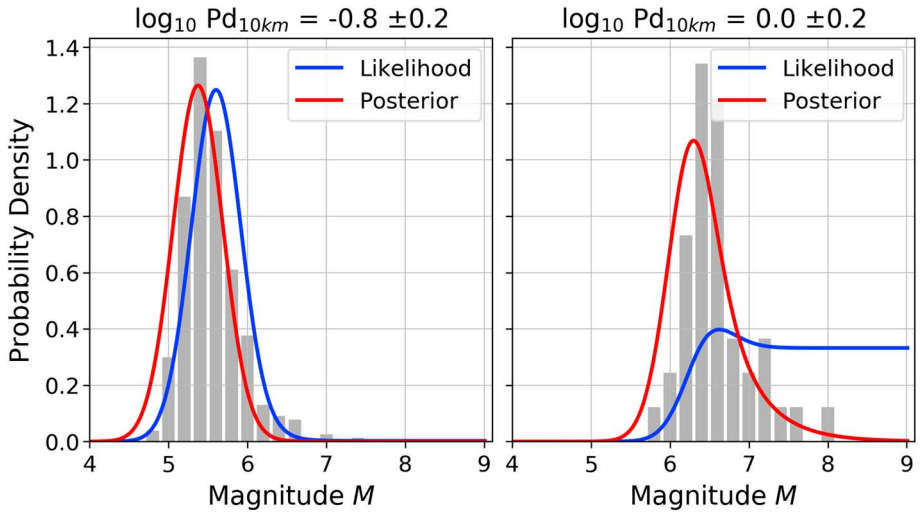

Figure 8. Comparison of the likelihood function (blue curve) and posterior probability distribution (red curve) for a fixed 3-s measurement time window *TW*. The left panel corresponds to $\log_{10}P_d = -0.8 \pm 0.2$, which is below the saturation point given by (4) for a 3-s *TW*, while the right panel corresponds to $\log_{10}P_d = 0.0 \pm 0.2$, which is slightly above the saturation point. The underlying magnitude histograms from our data set are shown for reference.

P_d-based magnitude estimates are an integral component of network EEW systems like ShakeAlert. Since P_d gives a snapshot of the evolving magnitude, these magnitude estimates can be highly informative provided *TW* exceeds T_{rup}. It may however be worth exploring further how best to process real-time seismic datastreams in order to reliably compute P_d. For consistency with previous work, we measure P_d from doubly integrated acceleration waveforms that have been filtered in the 0.075- to 3.0-Hz band. Visual examination of these derived displacement waveforms suggests that there may be significant artifacts inherent to the double-integration process, particularly during dense aftershock sequences where long-period noise and residual tilts in the accelerometer are not adequately removed by the application of high-pass filter at 0.075 Hz. A potential solution for more accurate estimates may be to incorporate geodetic data, which is currently being explored for the ShakeAlert system (Murray et al., 2018). While beyond the scope of this study, the Bayesian framework we develop here should in principle be applicable to compute time-dependent uncertainties in geodetic EEW systems, which can reliably measure the peak static and dynamic ground displacement but issue significantly slower alerts due to their dependence on *S* waveform data. Alternatively, EEW systems may be able to accurately forecast strong shaking from seismic data without requiring accurate displacement measurements using methods that estimate the extent of the rupture, such as FinDer (Böse et al., 2012), or by issuing alerts directly from observed ground motion without directly solving for source properties (Hoshiba & Aoki, 2015).

The question of rupture determinism remains crucial to our understanding of earthquake rupture processes. With the development and application of machine learning and other advanced statistical techniques, it is possible that we may uncover hidden features of seismic or geodetic waveforms that are capable of producing deterministic forecasts of earthquake magnitude using very limited snapshots of data. Our measurements of P_d spanning a wide range of earthquake magnitudes do not appear to support rupture determinism, at least in its strong form. Colombelli et al. (2014), for example, observe a slower initial growth in P_d for large earthquakes, but as exemplified by Figure 6, this behavior would be difficult to discern in real time. A weaker form of determinism in which the final earthquake size correlates with slip pulse behavior after several tens of seconds (Goldberg et al., 2019; Melgar & Hayes, 2017) is quite plausible but remains beyond the resolution of P_d measurements made from *P* waveforms alone. Careful analyses of near-source recordings that image pulse-like rupture behavior may yield insight into the fundamental question of rupture determinism but will have limited applicability to EEW systems as presently constructed. Until more scientific progress is made in this realm, EEW systems like ShakeAlert that rely on *P* wave P_d measurements should operate under a more cautious assumption of nondeterministic rupture and work to incorporate time-dependent magnitude uncertainties into probabilistic shaking forecasts. The March 2011 M9 Tohoku-oki earthquake provides a particularly sobering example in this regard. If one examines waveform amplitudes within a

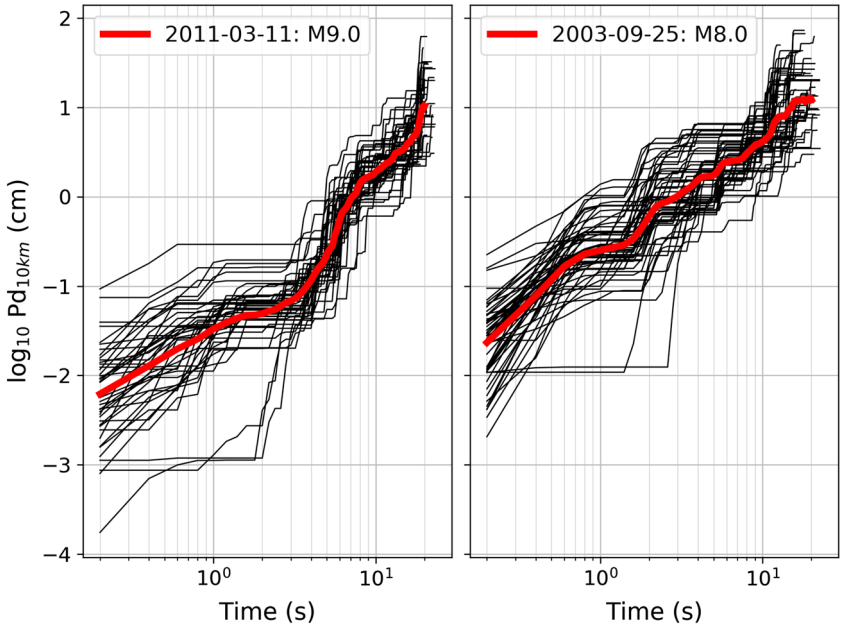

Figure 9. Comparison of the time evolution of peak displacement for the two largest earthquakes in our data set: the 2011 M9.0 Tohoku-oki and the 2003 M8.0 Tokachi-oki earthquakes. Distance-normalized P_d measurements from individual records are plotted versus time on a log-log scale (thin black lines), with event averages overlain (thick red lines). The Tohoku-oki earthquake (left) begins with weak initial growth in P_d in the first 4 s after onset before a stage of rapid increase P_d. In contrast, the Tokachi-oki earthquake (right) exhibits a more consistent growth in P_d.

short time window following P wave onset, there is little hint that the earthquake will grow into one of the largest in recorded history (Figure 9). While Tohoku-oki is well-known for its rapid moment release (Chounet & Vallée, 2018; Minson et al., 2014), this does not become apparent in the displacement waveforms until at least 4 s after onset, and indeed the normalized displacement amplitudes are significantly less than those of the 2003 M8 Tokachi-oki event until much later in the rupture process. Whether this slow initial growth is peculiar to the Tohoku-oki earthquake or is common for other great earthquakes remains an open question. But it is an instructive reminder that the first few seconds of rupture may not determine the final earthquake size.

5. Summary

We study the relation between P wave peak displacement P_d and magnitude M for a large data set of M4.5–9.0 earthquakes recorded by the Japanese K-NET and KiK-net strong-motion networks. The time evolution of P_d for earthquakes in our data set suggests a universal pattern of initial growth that is inconsistent with deterministic models of earthquake rupture. We demonstrate that there is a magnitude-dependent saturation in the linear $\log_{10}P_d$-M relation assumed in many EEW systems that is well-explained by a simple, nondeterministic model of earthquake rupture with constant rupture velocity. When combined with the observation that within-event and between-event variability in $\log_{10}P_d$ are normally distributed, this saturation model provides a basis for a rapid, analytic Bayesian method for calculating uncertainties in the displacement-based magnitude estimates that are central to many EEW systems.

Acknowledgments
We gratefully acknowledge use of K-NET and KiK-net strong-motion waveform data made available by the Japanese National Research Institute for Earth Science and Disaster Resilience (NIED; http://www.kyoshin.bosai.go.jp/, last accessed 08 February 2019). Waveform processing was performed using the ObsPy toolkit (Beyreuther et al., 2010). Peak displacement measurement data and associated waveform metadata are listed in Data Set S1. We are thankful for feedback from internal reviewers J. Gomberg and J. Murray, J. Vidale, and an anonymous peer reviewer, as well as the associate editor, all of whose thoughtful comments and suggestions improved the manuscript. We also thank M. Meier for his keen insight and helpful scientific discussions. D. Trugman acknowledges institutional support from the Laboratory Directed Research and Development (LDRD) program of Los Alamos National Laboratory under project 20180700PRD1.

References

Aki, K. (1967). Scaling law of seismic spectrum. *Journal of Geophysical Research*, *72*(4), 1217–1231. https://doi.org/10.1029/JZ072i004p01217

Aki, K., & Richards, P. G. (2002). *Quantitative seismology* (2nd ed.). Sausalito, CA: University Science Books.

Allen, R. V. (1978). Automatic earthquake recognition and timing from single traces. *Bulletin of the Seismological Society of America*, *68*(5), 1521–1532.

Allen, R. M., & Kanamori, H. (2003). The potential for earthquake early warning in Southern California. *Science*, *300*(5620), 786–789. https://doi.org/10.1126/science.1080912

Allmann, B. P., & Shearer, P. M. (2009). Global variations of stress drop for moderate to large earthquakes. *Journal of Geophysical Research*, *114*, B01310. https://doi.org/10.1029/2008JB005821

Beyreuther, M., Barsch, R., Krischer, L., Megies, T., Behr, Y., & Wassermann, J. (2010). ObsPy: A python toolbox for seismology. *Seismological Research Letters*, *81*(3), 530–533. https://doi.org/10.1785/gssrl.81.3.530

Böse, M., Heaton, T. H., & Hauksson, E. (2012). Real-time finite fault rupture detector (FinDer) for large earthquakes. *Geophysical Journal International*, *191*, 803–812. https://doi.org/10.1111/j.1365-246X.2012.05657.x

Brodsky, E. E., & Kanamori, H. (2001). Elastohydrodynamic lubrication of faults. *Journal of Geophysical Research*, *106*(B8), 16,357–16,374. https://doi.org/10.1029/2001JB000430

Brown, H. M., Allen, R. M., Hellweg, M., Khainovski, O., Neuhauser, D., & Souf, A. (2011). Development of the ElarmS methodology for earthquake early warning: Realtime application in California and offline testing in Japan. *Soil Dynamics and Earthquake Engineering*, *31*(2), 188–200. https://doi.org/10.1016/j.soildyn.2010.03.008

Brune, J. N. (1970). Tectonic stress and the spectra of seismic shear waves from earthquakes. *Journal of Geophysical Research*, *75*(26), 4997–5009. https://doi.org/10.1029/JB075i026p04997

Chounet, A., & Vallée, M. (2018). Global and interregion characterization of subduction interface earthquakes derived from source time functions properties. *Journal of Geophysical Research: Solid Earth*, *123*, 5831–5852. https://doi.org/10.1029/2018JB015932

Chung, A. I., Henson, I., & Allen, R. M. (2019). Optimizing earthquake early warning performance: ElarmS3. *Seismological Research Letters*, *90*(2), 463–466. https://doi.org/10.1785/0220180192

Cochran, E. S., Kohler, M. D., Given, D. D., Guiwits, S., Andrews, J., Meier, M.-A., et al. (2018). Earthquake early warning shakealert system: Testing and certification platform. *Seismological Research Letters*, *89*(1), 108–117. https://doi.org/10.1785/0220170138

Colombelli, S., Zollo, A., Festa, G., & Kanamori, H. (2012). Early magnitude and potential damage zone estimates for the great Mw 9 Tohoku-Oki earthquake. *Geophysical Research Letters*, *39*, L22306. https://doi.org/10.1029/2012GL053923

Colombelli, S., Zollo, A., Festa, G., & Picozzi, M. (2014). Evidence for a difference in rupture initiation between small and large earthquakes. *Nature Communications*, *5*, 3958. https://doi.org/10.1038/ncomms4958

Crowell, B. W., Bock, Y., & Melgar, D. (2012). Realtime inversion of GPS data for finite fault modeling and rapid hazard assessment. *Geophysical Research Letters*, *39*, L09305. https://doi.org/10.1029/2012GL051318

Denolle, M. A., & Shearer, P. M. (2016). New perspectives on self-similarity for shallow thrust earthquakes. *Journal of Geophysical Research: Solid Earth*, *121*, 6533–6565. https://doi.org/10.1002/2016JB013105

Ellsworth, W. L., & Beroza, G. C. (1995). Seismic evidence for an earthquake nucleation phase. *Science*, *268*(5212), 851–855. https://doi.org/10.1126/science.268.5212.851

Eshelby, J. D. (1957). The determination of the elastic field of an ellipsoidal inclusion, and related problems. *Proceedings of the Royal Society A: Mathematical, Physical and Engineering Sciences*, *241*(1226), 376–396. https://doi.org/10.1098/rspa.1957.0133

Goldberg, D. E., Melgar, D., Bock, Y., & Allen, R. M. (2019). Geodetic observations of weak determinism in rupture evolution of large earthquakes. *Journal of Geophysical Research: Solid Earth*, *123*, 9950–9962. https://doi.org/10.1029/2018JB015962

Goldsby, D. L., & Tullis, T. E. (2011). Flash heating leads to low frictional strength of crustal rocks at earthquake slip rates. *Science*, *334*(6053), 216–218. https://doi.org/10.1126/science.1207902

Gomberg, J., Wech, A., Creager, K., Obara, K., & Agnew, D. (2016). Reconsidering earthquake scaling. *Geophysical Research Letters*, *43*, 6243–6251. https://doi.org/10.1002/2016GL069967

Heaton, T. H. (1990). Evidence for and implications of self-healing pulses of slip in earthquake rupture. *Physics of the Earth and Planetary Interiors*, *64*(1), 1–20. https://doi.org/10.1016/0031-9201(90)90002-F

Hoshiba, M., & Aoki, S. (2015). Numerical shake prediction for earthquake early warning: Data assimilation, realtime shake mapping, and simulation of wave propagation. *Bulletin of the Seismological Society of America*, *105*(3), 1324–1338. https://doi.org/10.1785/0120140280

Hoshiba, M., & Iwakiri, K. (2011). Initial 30 seconds of the 2011 off the Pacific coast of Tohoku earthquake (M9.0): Amplitude and τ_c for magnitude estimation for earthquake early warning. *Earth, Planets and Space*, *63*(7), 8. https://doi.org/10.5047/eps.2011.06.015

Ide, S., & Beroza, G. C. (2001). Does apparent stress vary with earthquake size? *Geophysical Research Letters*, *28*(17), 3349–3352. https://doi.org/10.1029/2001GL013106

Kanamori, H. (2005). Real-time seismology and earthquake damage mitigation. *Annual Review of Earth and Planetary Sciences*, *33*(1), 195–214. https://doi.org/10.1146/annurev.earth.33.092203.122626

Kohler, M. D., Cochran, E. S., Given, D., Guiwits, S., Neuhauser, D., Henson, I., et al. (2018). Earthquake early warning shakealert system: West coast wide production prototype. *Seismological Research Letters*, *89*(1), 99–107. https://doi.org/10.1785/0220170140

Kuyuk, H. S., & Allen, R. M. (2013). A global approach to provide magnitude estimates for earthquake early warning alerts. *Geophysical Research Letters*, *40*, 6329–6333. https://doi.org/10.1002/2013GL058580

Kuyuk, H. S., Allen, R. M., Brown, H., Hellweg, M., Henson, I., & Neuhauser, D. (2014). Designing a network-based earthquake early warning algorithm for California: ElarmS-2. *Bulletin of the Seismological Society of America*, *104*(1), 162–173. https://doi.org/10.1785/0120130146

Leyton, F., Ruiz, S., Baez, J. C., Meneses, G., & Madariaga, R. (2018). How fast can we reliably estimate the magnitude of subduction earthquakes? *Geophysical Research Letters*, *45*, 9633–9641. https://doi.org/10.1029/2018GL078991

Madariaga, R. (1978). The dynamic field of Haskell's rectangular dislocation fault model. *Bulletin of the Seismological Society of America*, *68*(4), 869–887.

Meier, M.-A. (2017). How good are real-time ground motion predictions from earthquake early warning systems? *Journal of Geophysical Research: Solid Earth*, *122*, 5561–5577. https://doi.org/10.1002/2017JB014025

Meier, M.-A., Ampuero, J. P., & Heaton, T. H. (2017). The hidden simplicity of subduction megathrust earthquakes. *Science*, *357*(6357), 1277–1281. https://doi.org/10.1126/science.aan5643

Meier, M.-A., Heaton, T., & Clinton, J. (2016). Evidence for universal earthquake rupture initiation behavior. *Geophysical Research Letters*, *43*, 7991–7996. https://doi.org/10.1002/2016GL070081

Melgar, D., Bock, Y., Sanchez, D., & Crowell, B. W. (2013). On robust and reliable automated baseline corrections for strong motion seismology. *Journal of Geophysical Research: Solid Earth*, *118*, 1177–1187. https://doi.org/10.1002/jgrb.50135

Melgar, D., & Hayes, G. P. (2017). Systematic observations of the slip pulse properties of large earthquake ruptures. *Geophysical Research Letters*, *44*, 9691–9698. https://doi.org/10.1002/2017GL074916

Minson, S. E., Meier, M.-A., Baltay, A. S., Hanks, T. C., & Cochran, E. S. (2018). The limits of earthquake early warning: Timeliness of ground motion estimates. *Science Advances*, *4*(3), eaaq0504. https://doi.org/10.1126/sciadv.aaq0504

Minson, S. E., Simons, M., Beck, J. L., Ortega, F., Jiang, J., Owen, S. E., et al. (2014). Bayesian inversion for finite fault earthquake source models II: The 2011 great Tohoku-oki, Japan earthquake. *Geophysical Journal International*, *198*(2), 922–940. https://doi.org/10.1093/gji/ggu170

Murray, J. R., Crowell, B. W., Grapenthin, R., Hodgkinson, K., Langbein, J. O., Melbourne, T., et al. (2018). Development of a geodetic component for the U.S. West Coast earthquake early warning system. *Seismological Research Letters*, *89*(6), 2322–2336. https://doi.org/10.1785/0220180162

Nielsen, S. (2007). Can earthquake size be controlled by the initial seconds of rupture? *Earthquake early warning systems* (pp. 9–20). Berlin, Heidelberg: Springer.

Noda, H., & Lapusta, N. (2013). Stable creeping fault segments can become destructive as a result of dynamic weakening. *Nature*, *493*(7433), 518–521. https://doi.org/10.1038/nature11703

Nof, R. N., & Allen, R. M. (2016). Implementing the elarms earthquake early warning algorithm on the Israeli seismic network. *Bulletin of the Seismological Society of America*, *106*(5), 2332–2344. https://doi.org/10.1785/0120160010

Olson, E. L., & Allen, R. M. (2005). The deterministic nature of earthquake rupture. *Nature*, *438*(7065), 212–215. https://doi.org/10.1038/nature04214

Olson, E. L., & Allen, R. M. (2006). Earth science: Is earthquake rupture deterministic? (Reply). *Nature*, *442*(7100), E6. https://doi.org/10.1038/nature04964

Rydelek, P., & Horiuchi, S. (2006). Earth science: Is earthquake rupture deterministic? *Nature*, *442*(7100), E5–E6. https://doi.org/10.1038/nature04963

Rydelek, P., Wu, C., & Horiuchi, S. (2007). Comment on Earthquake magnitude estimation from peak amplitudes of very early seismic signals on strong motion records by Aldo Zollo, Maria Lancieri, and Stefan Nielsen. *Geophysical Research Letters*, *34*, L20302. https://doi.org/10.1029/2007GL029387

Trugman, D. T., & Shearer, P. M. (2017). Application of an improved spectral decomposition method to examine earthquake source scaling in southern California. *Journal of Geophysical Research: Solid Earth*, *122*, 2890–2910. https://doi.org/10.1002/2017JB013971

Ueno, H., Hatakeyama, S., Aketagawa, T., Funasaki, J., & Hamada, N. (2002). Improvement of hypocenter determination procedures in the Japan Meteorological Agency. *Quarterly Journal of Seismology*, *65*(1-4), 123–134.

Yamada, T., & Ide, S. (2008). Limitation of the predominant-period estimator for earthquake early warning and the initial rupture of earthquakes. *Bulletin of the Seismological Society of America*, *98*(6), 2739–2745. https://doi.org/10.1785/0120080144

Ye, L., Lay, T., Kanamori, H., & Rivera, L. (2016). Rupture characteristics of major and great (M>=7.0) megathrust earthquakes from 1990 to 2015: 1. Source parameter scaling relationships. *Journal of Geophysical Research: Solid Earth*, *121*, 826–844. https://doi.org/10.1002/2015JB012426

Zollo, A., Lancieri, M., & Nielsen, S. (2006). Earthquake magnitude estimation from peak amplitudes of very early seismic signals on strong motion records. *Geophysical Research Letters*, *33*, L23312. https://doi.org/10.1029/2006GL027795